Improvement of thermal conductivity by adding tungsten and/or copper wire in F82H

Jeongwoo Heo[1], N. Hashimoto[2], H. Oka[2], H. Noto[3]

[1] *Graduate School of Engineering, Hokkaido University, Sapporo, 060-8628 Japan*

[2] *Faculty of Engineering, Hokkaido University, Sapporo, 060-8628 Japan*

[3] *National Institute for Fusion Science, 322-6 Oroshi-cho, Toki, Gifu 509-5292, Japan*

Abstract

The F82H, which is one of reduced activation ferritic/martensitic steels, is a strong candidate structure material for fusion reactor because of its good mechanical property and high swelling resistance in the operating temperature range. One of disadvantage of F82H would be its low thermal conductivity as a structure material for divertor. In this study, we have fabricated several F82H-based composite materials by the spark plasma sintering in order to improve its thermal conductivity by adding tungsten and/or copper wires. F82H-20 vol.% W and F82H-10 vol.% W-10 vol.% Cu composites included reaction layer at the interface between tungsten wire and F82H matrix, resulted in the decrease in ductility and tensile strength due to the formation of tungsten carbide. On the other hand, F82H-20 vol.% Cu composite, sintered for 120 min at 1000 °C, included no reaction layers and showed the highest thermal conductivity with a high relative density. Furthermore, this composite indicated a great tensile property, which is comparable to that of the original F82H.

1. Introduction

The RAFM (Reduced Activation Ferritic / Martensitic) steel is one of candidate materials for the plasma facing components (PFCs) in the nuclear fusion reactor due to its high resistance against the neutron radiation condition [1-3]. On the other hand, the structural materials in the coolant system and the divertor should have enough thermal conductivity as a heat transfer from the

plasma faced region to the coolant [4]. The RAFM steel have good mechanical properties at high temperature and the excellent swelling resistance, however, the thermal conductivity of the RAFM is not enough as a divertor material compared with the other candidate materials such as tungsten-based or copper-based alloys [5-9]. In this study, therefore, we designed a RAFM steel-metal composite materials in order to improve the thermal conductivity of the RAFM steels. The increase in thermal conductivities of the composites could be expected with the addition of metal wires which have a high thermal conductivity such as pure copper (401 W/(m•k)) and pure tungsten (173 W/(m•k)) [9-12]. The advantages of using tungsten are its low coefficient of thermal expansion (CTE), low neutron activation, low tritium retention and so on [13]. However, one of problems would be the difference of CTE between tungsten (4.3×10^{-6}/K) and F82H (12×10^{-6}/K). It could lead to the mechanical failure due to the thermal mismatch and the dimensional instability during operation at variable temperature [9, 14-16].

2. Experiments

F82H powders, tungsten wires (Nippon Tungsten CO., LTD, 99.96% or higher purity), and copper wires (Nilaco Co., 99.9% purity) are used in this study. The typical compositions of F82H are listed in Table 1. The sizes of F82H powders (~125 μmϕ) were made by gas atomization from the bulk. The F82H powders were sintered with tungsten wires and copper wires (1 mm in length and 300 μm in diameter). All the composites were sintered by Spark Plasma Sintering (SPS: DR.SINTER.LAB, SPS+510 L). In each SPS holder, tungsten and copper wires were stuck into the F82H powder. The direction of wires was perpendicular to the compression direction for the sintering. The composites were sintered as the metal volume fraction of F82H-xW-yCu (x, y = 0~20 vol%). The SPS was conducted at the heating rate of 100 °C/min from room temperature to 750°C, and then, 50°C/min up to 1000 °C under the pressure of 40 MPa. The holding time at the

highest temperature was 10, 60, and 120 min, respectively. Figure 1 (a) shows the temperature profile applied during the SPS process. The conceptual model for our study is depicted as shown in Figure 1 (b). The size of SPSed specimens is 20 mm diameters and the height is 10 mm. SPSed specimens were cut and machined into a cylinder disc about 10 mm diameters and 2 mm height from the vertical direction, and then, the surface of each specimens was polished using paper with grits 800, 1000, and 2000 for 6 min, respectively. After cutting and polishing, stress-relief annealing in vacuum was performed at temperature of 800 °C for 180 min to reduce the inner stress of the specimens.

The relative density and the thermal diffusivity of F82H-*x*W-*y*Cu composites were measured by the Archimedes method and the Laser Flash Apparatus (Netzsch, LFA 457 MicroFlash), respectively. The direction of the heat flux during LFA was in the direct path of wires in the F82H matrix. The thermal conductivity of each specimen was calculated by using the thermal diffusivity and specific heat data. The specific thermal conductivity could be calculated using the equation of thermal diffusivity:

$$\lambda = \alpha \times C_p \times \rho$$

where λ is the specific thermal conductivity, α is the thermal diffusivity, C_ρ is the specific heat, and ρ is the density [17].

To observe the precipitates and grain boundaries of the surface on F82H-20Cu composite with 120 min SPS holding time, the surface of fabricated 3mmΦ disk specimens was electro polished using a mixed solution of 5% perchloric acid and 95% ethanol. The prepared specimen was observed for microstructure and precipitate using SEM. In addition, in order to observe the microstructure change on the specimens produced according to the thermal history, a TEM sample was prepared using a focused ion beam (FIB, HITACHI, FB-2100) for the F82H-Cu interface of the F82H-20Cu composite material, and then the cross section observation was performed using

a transmission electron microscope (TEM, JEOL, JEM-2010).

Mechanical properties were investigated by tensile test (Instron-5564). The surface structure in the tip of tensile-tested F82H-*x*W-*y*Cu composites were also investigated by using a scanning electron microscope (SEM, JEOL, JSM-6510LA) and an energy dispersive spectroscopy (EDS, JEOL, JED-2300). Furthermore, the EDS mapping was carried out around the deformed area of tensile-tested samples.

3. ***Results***

The expected thermal conductivity of a composite was estimated on a basis of the mixture rule [18]. In general, the mixture rule on a thermal conductivity of a composite is expressed as below:

$$\lambda_{\text{composite}} = \lambda_{\text{matrix}} V_{\text{matrix}} + \lambda_{\text{additive}} V_{\text{additive}}$$

The expected thermal conductivity of the composite, $\lambda_{\text{composite}}$ is the sum of thermal conductivity of the matrix and thermal conductivity of the additive which is directly proportionate to each volume fraction. When a composite is fully dense, it could show their highest thermal conductivity. The expected thermal conductivities of all composites are shown in Table 2. And the actual thermal conductivities and the relative densities of the composites were summarized and listed in Fig. 2 and Table 2 Basically, the actual thermal conductivity of a composite would be lower than the expected value calculated by the formula of the mixture rule. The theoretical value of the thermal conductivity of F82H-20Cu composite is 105.2 W/(m•k), while the actual thermal conductivity of F82H-20Cu composite with 120 min SPS holding time was 103.0 W/(m•k) probably due to less relative density by sintering. The highest thermal conductivity was three times higher compared with general F82H (31.3 W/(m•k)). Fig. 3(a)–(i) show surface structures of F82H-20Cu, F82H-10W-10Cu and F82H-20W composites with 10 to 120 min SPS holding time. In aspect of the SPS holding time, the thermal conductivity increases as the relative density

increases. Cu wires became softer and were shaped like flakes at the longer sintering time. As indicated by arrows in Fig. 3(a), (d) and (g), the diverse and multitudinous pores were formed in F82H matrix. In the case of 10 min SPS holding time, F82H powder with spherical shape was found probably due to less holding time. The number of pores tends to be decreased with increasing SPS holding time. For example, in the case of 60 min holding time, the number of pores has decreased compared to that of 10 min holding time. The pores finally disappeared in the SPS condition of 120 minutes.

The composite shown in Fig. 4(a)–(c) is F82H-20Cu composite SPSed at 1000 ºC for 120 min. Fig. 4(a) and (b) show etched surface of F82H-20Cu composite. $M_{23}C_6$ carbides at the grain, packet and lath boundaries were indicated by yellow arrows and fine MX precipitates were indicated by white arrows in fig. 4(b). As shown in fig (c), TEM observation was performed for cross-section observation. There is a surface of the specimen in the upper left-hand corner. The FIB milled copper wire is in the lower left side. And at the right side, F82H matrix with Prior austenite grain boundaries, packet and lath boundaries was observed.

The engineering stress-strain curves of the composites are depicted in Figure 5. The 0.2% offset yield stress, ultimate tensile strength and total elongation of each composite are listed in Table 3. All the tensile-tested specimens failed in the mid-substance. F82H-20W composite material with 120 min SPS holding time showed the highest ultimate tensile stress of 605.9 MPa. The highest engineering strain (the total elongation of 17.7 %) was seen in the F82H-20Cu composite material with 120 min SPS holding time, which statistically greater than F82H-20W and F82H-10W-10Cu. In order to investigate the fracture mode of each composite, SEM observation was performed for the tip of the tensile-tested specimens. Fig. 6(a)–(c), 6(d)–(f), and 6(g)–(h) show SEM images of the tip of the tensile-tested F82H-20W, F82H-10W-10Cu, and F82H-20Cu composites with 120 min SPS holding time, respectively. From the SEM images, it is recognized that F82H-20W and

F82H-10W-10Cu were deformed with phase separation at the interface between W-wire and F82H matrix. On the other hand, F82H-20Cu showed no phase separation but the deformation with necking. While the fracture surface of F82H area showed dimple structure as shown with yellow circles in Fig. 6(a), 6(d) and 6(g). The EDS mapping performed for the tip of the tensile-tested F82H-20Cu (Fig. 6(i)) indicated that the interface between copper-wire and F82H matrix would be stable even after the deformation.

4. Discussion

One of purposes in this study is the optimization of the SPS condition and the value of (x, y) in F82H-xW-yCu composites on a basis of the higher thermal conductivity. As listed in Table 2, the composite including larger amount of copper showed higher thermal conductivity than tungsten-including composites. In accordance with these results, the amount of copper wire would be more effective for the increase in the thermal conductivity than tungsten wire. Therefore, in the aspect of thermal conductivity, the best value of (x, y) would be (0, 20) in this study. Furthermore, despite the SPS was performed at temperature of 1000 °C for 120 min, the microstructural modifications were not observed. In Fig. 4(a)–(c), it showed F82H-based composite could have typical lath martensite structure with $M_{23}C_6$ carbides at the grain, packet and lath boundaries and nano-scale MX precipitates in laths.

On the other hand, the formation of pores in sintered materials is a very critical issue because it would degrade the thermal conductivity and the tensile property due to the decrease in relative density. Actually, in this study, the decrease in relative density resulted in the decrease in thermal conductivity. According to SEM observation, the number of pores in sintered composites was decreased with longer holding time. At last, the sintering with 120 min SPS holding time resulted in no formation of pore in matrix. Hence, a longer SPS holding time (> 120 min) would be

effective to make F82H-20Cu composite a denser and a higher thermal conductivity material.

In addition, the interface between tungsten-, copper wire and F82H would act an important role to its tensile property Total elongation (TE), the yield stress (YS), and the ultimate tensile strength (UTS) of the general F82H steel are 21.7 %, 548 MPa and 669 MPa, respectively [9]. However, the sintered composites resulted in the decrease in the tensile properties compared to general F82H as shown in Fig. 5. In terms of F82H-20W composite with 120 min SPS holding time, the 0.2 % proof stress and the UTS were the highest, while the TE was the worst among the composites. As shown in Fig. 6, the separation of tungsten wire from F82H matrix was observed in F82H-20W and F82H-10W-10Cu. This would be due to the formation of the reaction layer or intermetallic compounds at the interface between tungsten wire and F82H during sintering It was reported that the reaction layer and the diffusion layer in F82H-W wire composite material [19]. Basically, tungsten and ferritic steel have differences in their coefficients of thermal expansion [20], melting temperature, and elasticity modulus [21], so that, the rapid temperature change would generate high internal stresses, leading to separation or failure [22]. In addition, it was reported that the formation of intermetallic compounds such as Fe_7W_6, Fe_3W_3C and Fe_2W phases could be found between tungsten and matrix in sintered steels [23]. From our previous report [19], it is suggested that Fe_2W intermetallic compound formation would occur in this study. The formation of intermetallic compounds at the interface between matrix and W wires would degrade the mechanical property of the sintered composites because it could be a source of crack initiation during deformation. In actual, those tungsten wires in F82H-20W and F82H-10W-10Cu were pulled out from the F82H matrix during tensile testing as shown in Fig. 6. On the other hand, F82H-20Cu showed no separation and/or crack initiation at the interface between copper wire and F82H matrix, resulted in a comparable tensile property. From those results, it is suggested that the optimized condition to improve the thermal conductivity of F82H-based composite would be

F82H-20Cu by sintering at 1000 ºC for 120 min, leading to a comparable tensile property with that of the original F82H.

5. Summary

F82H-based composite materials including tungsten and/or copper wires were fabricated in order to improve the thermal conductivity of general F82H. The results and the accomplishments were summarized as below:

• The increase in the amount of copper wire would be more effective to improve the thermal conductivity of F82H-based composite material compared with tungsten wire. This is probably due to no formation of reaction layer and tungsten carbide at the interface between wire and F82H matrix.

• The appropriate sintering condition for F82H-Cu composite would be at 1000 ºC for 120 min, leading to a higher density, a higher thermal conductivity, and a better tensile property. F82H-20Cu showed 3 times higher thermal conductivity and a comparable tensile property compared with that of general F82H.

Reference

[1] H. Wiedersich, J.J. Burton, J.L. Katz, Effect of mobile helium on void nucleation in materials during irradiation, Journal of Nuclear Materials, Vol.51, pp. 287, 1974

[2] M. Ando a, E. Wakai, T. Sawai, H. Tanigawa, K. Furuya, S. Jitsukawa, H. Takeuchi, K. Oka, S. Ohnuki, A. Kohyama, Synergistic effect of displacement damage and helium atoms on radiation hardening in F82H at TIARA facility, Journal of Nuclear Materials, Vol. 329, pp. 1137–1141, 2004

[3] S. J. Zinkle, Radiation-Induced Effects on Microstructure, Comprehensive Nuclear Materials, Vol. 1, pp. 65-98, 2012

[4] N. Hashimoto et al., Development of Fe-based composite materials for divertor by sintering with carbon nanotube, NuMat 2014, Clearwater, Florida, Oct. 27-30, 2014

[5] Smid I., Akiba M., Vieider G. and Plöchl L, Development of tungsten armor and bonding to copper for plasma-interactive components, Journal of Nuclear Materials Vol. 258 pp. 160, 1998

[6] Michael Rieth et al., Recent progress in research on tungsten materials for nuclear fusion applications in Europe, Journal of Nuclear Materials, Vol. 432, pp. 482-500, 2013

[7] G. J. Butterworth and C. B. A. Forty, A survey of the properties of copper alloys for use as fusion reactor materials, Journal of Nuclear Materials, vol. 189, no. 3, pp. 237–276, 1992

[8] H. Groh, D. Ellis, and W. Loewenthal, Comparison of GRCop-84 to other Cu alloys with high thermal conductivities, Journal of Materials Engineering and Performance, vol. 17, pp. 594–606, 2008

[9] K. Shiba, A. Hishinuma, A. Tohyama, K. Masamura, Properties of low activation ferritic steel F82H IEA heat, Japan Atomic Energy Research Institute Report JAERI-Tech 97-038, 1997

[10] Makinson, R. E. B. ,The thermal conductivity of metals, Mathematical Proceedings of the Cambridge Philosophical Society, Cambridge University Press Vol. 34 No.3, 1938

[11] N. Yamamouchi, M. Tamura, H. Hayakawa, A. Hishinuma, T. Kondo, Accumulation of engineering data for practical use of reduced activation ferritic steel: 8%Cr-2%W-0.2%V-0.04%Ta-Fe Journal of Nuclear Materials, Vol. 822, pp. 191-194, 1992

[12] K. Shiba, N. Yamanouchi, A. Tohyama, Preliminary results of the round-robin testing of F82H, Fusion materials semiannual progress report for the period ending June 30, 1996

[13] Ch. Linsmeier et al., Development of advanced high heat flux and plasma-facing materials, Nuclear Fusion, Volume 57, Number 9, 2017

[14] G. K. Horton, On the thermal expansion of metals at low temperatures, Canadian Journal of Physics, Vol. 39, 1961

[15] Theorie des festen Zustandes einatomiger Elemente, E. Grüneisen, Annalen der Phisik, Vol. 344, pp. 257, 1912

[16] Jayant S. Shah and M. E. Straumanis, Thermal Expansion of Tungsten at Low Temperatures, Journal of Applied Physics, Vol. 42, pp. 3288, 1971

[17] R. L. Hamilton, and O. K. Crosser, Thermal conductivity of heterogeneous two-component systems, Industrial & Engineering chemistry fundamentals 1.3, pp. 187-191, 1962

[18] C. J. Cremers, H. A. Fine, Thermal conductivity, Springer US, Vol. 21, 1990

[19] Z. Chen, Y. Sawa, and N. Hashimoto, Development of F82H composite materials with a high thermal conductivity, Nuclear materials and energy Vol. 16, pp. 133-136, 2018.

[20] B.A. Kalin, V.T. Fedotov, O.N. Sevrjukov, A.N. Kalashnikov, A.N. Suchkov, A. Moeslang, M. Rohde, J. Nucl. Mater. 367–370 (2007) 1218–1220.

[21] Q. Cai, W. Liu, Y. Ma, H. Liu, Int. J. Refract. Metals. Hard Mater. 48 (2015) 312–317.

[22] G. Cam, M. Kocak, Int. Mater. Rev. 43 (1998) 1–39.

[23] C. Tan, G. Wang, L. Ji, Y. Tong, X-M. Duan, J. Nucl. Mater. 469 (2016) 32–38.

Table 1 Chemical compositions of F82H

F82H	Fe	Cr	W	C	Si	Mn	V	Ta
(wt%)	Bal.	8.0	2.0	0.1	0.2	0.5	0.2	0.04

Table 2 Thermal conductivities and relative densities of composite materials

	SPS Holding Time [min]	**Expected thermal conductivity [W/(m•k)]**	**Actual thermal conductivity [W/(m•k)]**	**Relative density [%]**
F82H Bulk [9]	-	-	31.3	100
20W	10	59.8	55.5	99.5
20W	60	59.8	56.0	99.8
20W	120	59.8	58.5	99.9
10W-10Cu	10	82.5	74.4	98.9
10W-10Cu	60	82.5	75.7	99.4
10W-10Cu	120	82.5	81.2	99.8
20Cu	10	105.2	98.3	99.1
20Cu	60	105.2	100.9	99.3
20Cu	120	105.2	103.0	99.8

Table 3 Tensile properties of composite materials

ID [SPS holding time]	0.2% offset yield stress (Mpa)	Ultimate Strength (Mpa)	Total Elongation (%)
F82H[9]	548	669	21.7
20W [10 min]	7.2	18.3	1.3
20W [60 min]	497.6	464.0	2.4
20W [120 min]	514.4	605.9	2.5
10W-10Cu [10 min]	8.4	16.0	1.0
10W-10Cu [60 min]	384.3	428.9	6.8
10W-10Cu [120 min]	479.5	583.6	8.0
20Cu [10 min]	112.6	226.6	4.1
20Cu [60 min]	422.8	482.9	9.4
20Cu [120 min]	439.2	556.6	17.7

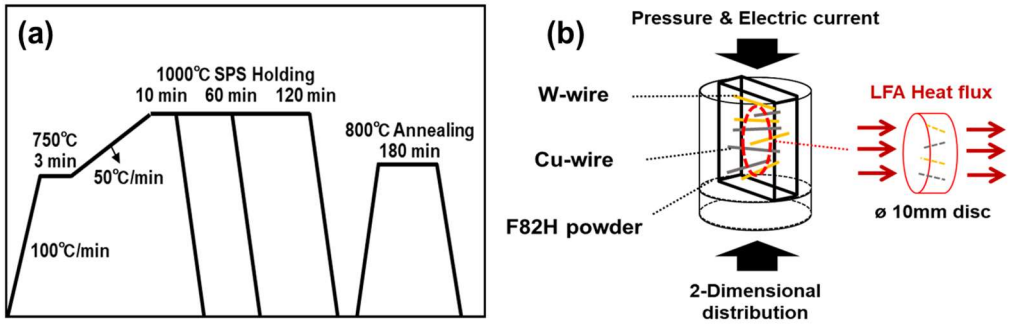

Fig. 1 (a) Temperature profile of the SPS and annealing process and (b) Conceptional model of experiments

0

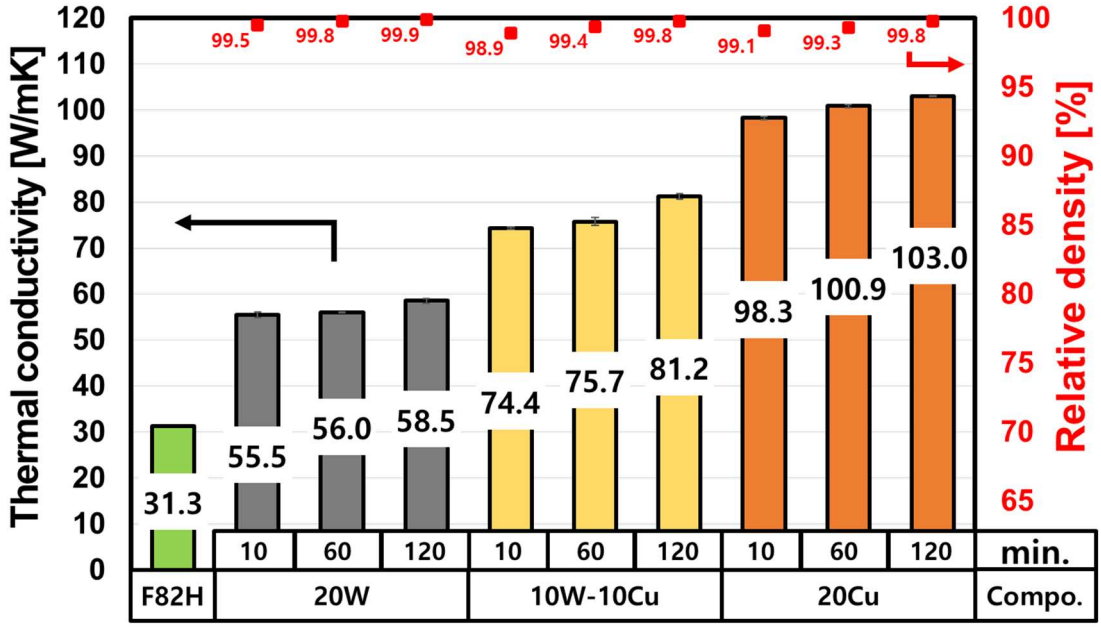

Fig. 2 Thermal conductivities and relative densities of F82H-*x*W-*y*Cu composites with diverse SPS conditions

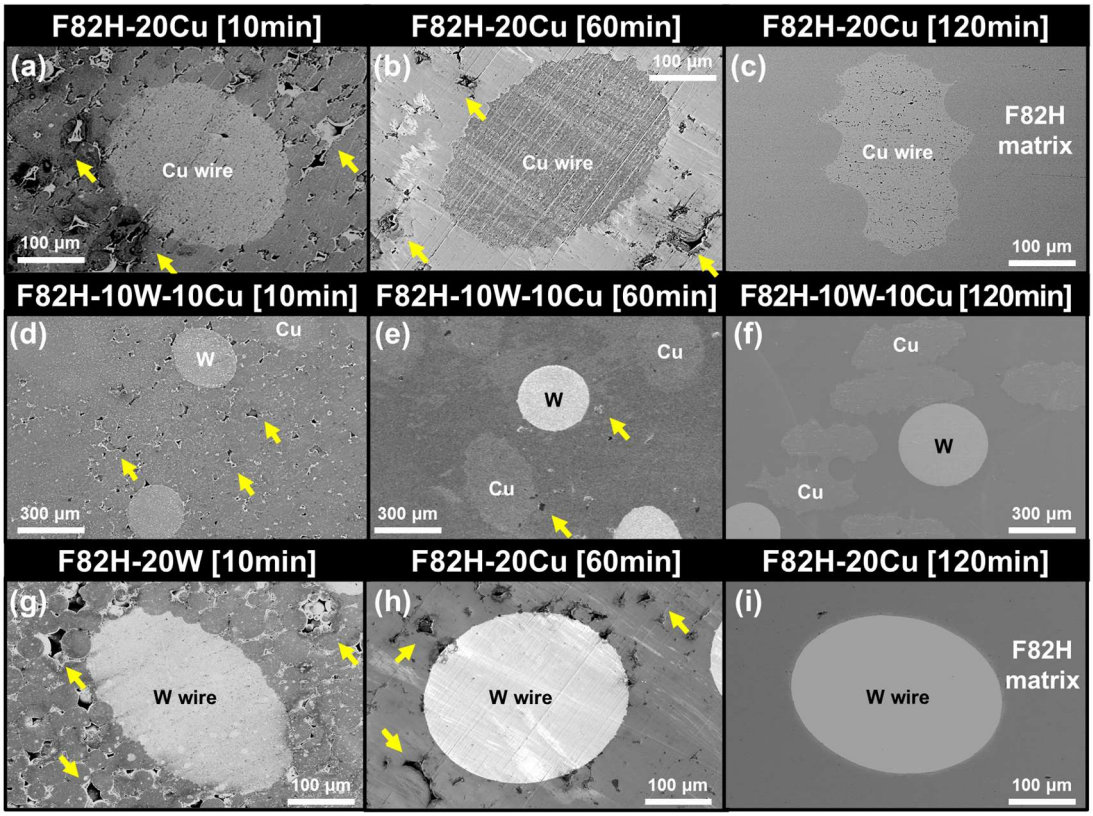

Fig. 3 Cross-sectional SEM images of F82H-20Cu, F82H-10W-10Cu and F82H-20W composites with 10 to 120 min SPS holding time

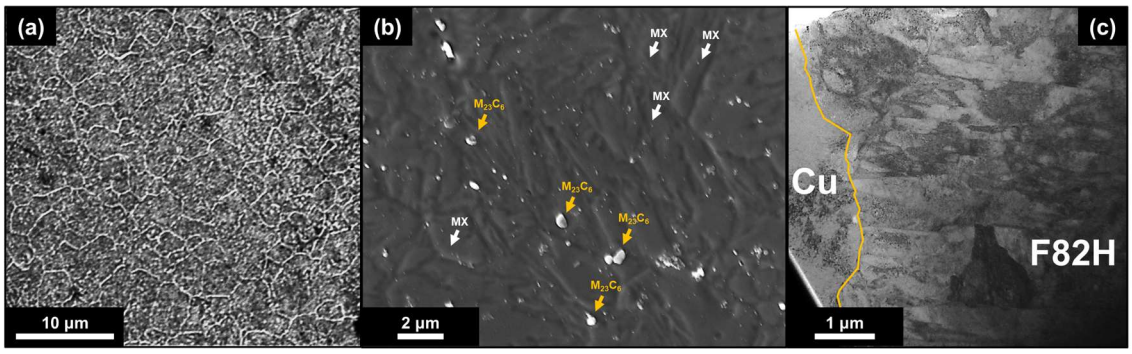

Fig. 4 (a), (b) SEM images of etched surface structures and (c) Cross-sectional TEM image on F82H-20Cu composite after SPS at 1000 °C for 120 min.

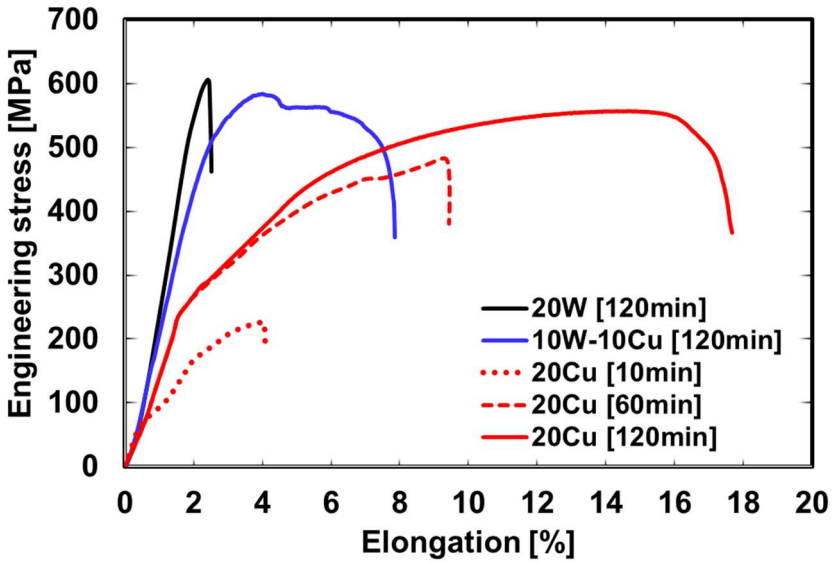

Fig. 5 Engineering stress-strain curves on F82H-based composites

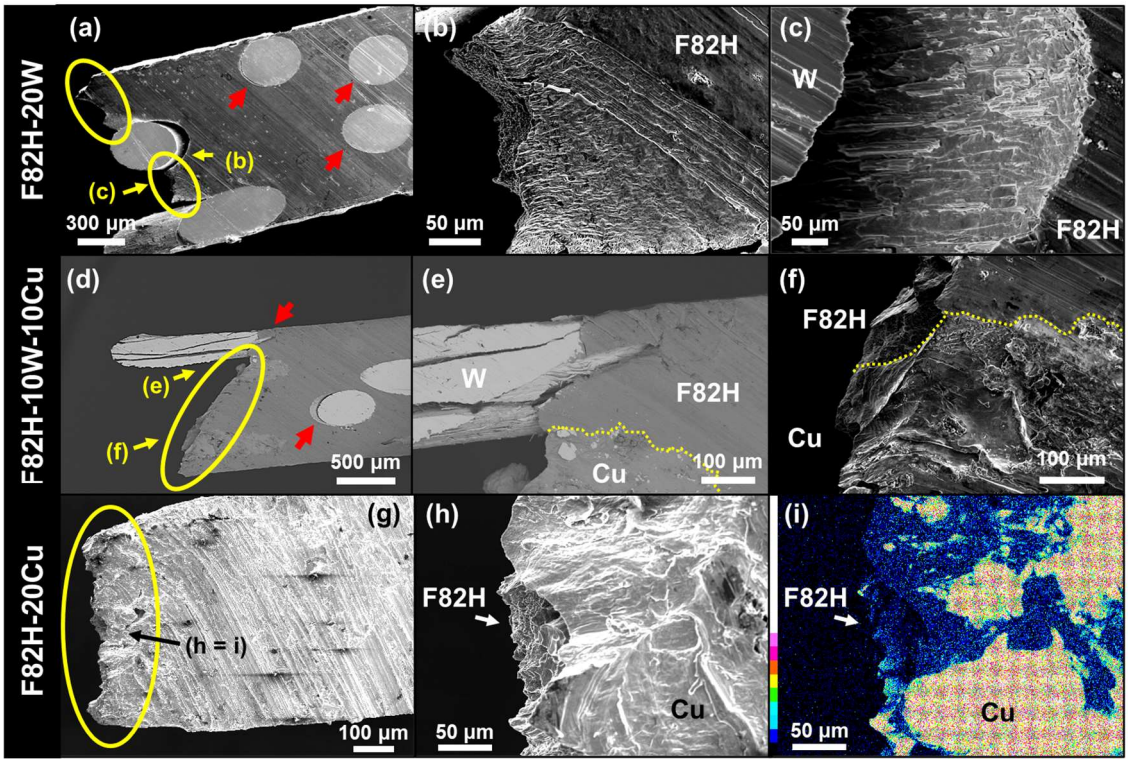

Fig. 6 SEM images and EDS mapping data of fracture surfaces on F82H-20W (a–c), F82H-10W-10Cu (d–f) and F82H-20Cu (g–h) composites with 120 min SPS holding time